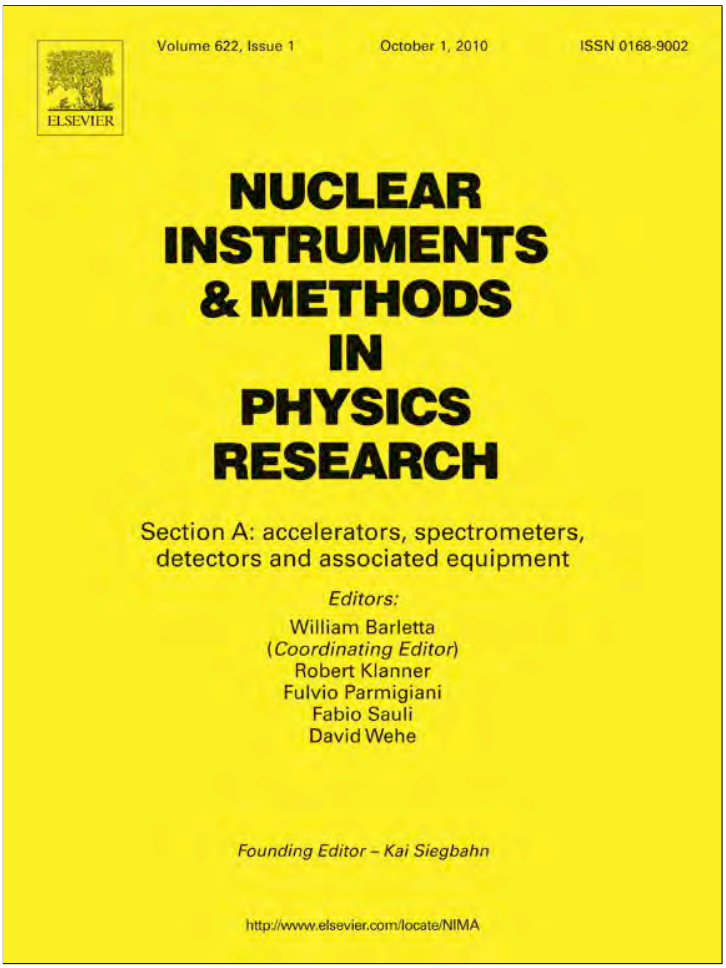

Nuclear Instruments and Methods in Physics Research A 622 (2010) 41–48

Contents lists available at ScienceDirect

Nuclear Instruments and Methods in Physics Research A

journal homepage: www.elsevier.com/locate/nima

A study of high-energy proton induced damage in cerium fluoride in comparison with measurements in lead tungstate calorimeter crystals

G. Dissertori [a], P. Lecomte [a], D. Luckey [a,1], F. Nessi-Tedaldi [a,*], F. Pauss [a], Th. Otto [b], S. Roesler [b], Ch. Urscheler [b]

[a] Institute for Particle Physics, ETH Zurich, 8093 Zurich, Switzerland
[b] CERN - DGS - RP Department, 1211 Geneva 23, Switzerland

ARTICLE INFO

Article history:
Received 10 May 2010
Received in revised form
7 July 2010
Accepted 15 July 2010
Available online 24 July 2010

Keywords:
Crystal calorimeter
Hadron damage
Scintillator

ABSTRACT

A CeF_3 crystal produced during early R&D studies for calorimetry at the CERN Large Hadron Collider was exposed to a 24 GeV/c proton fluence $\Phi_p = (2.78 \pm 0.20) \times 10^{13}\,cm^{-2}$ and, after one year of measurements tracking its recovery, to a fluence $\Phi_p = (2.12 \pm 0.15) \times 10^{14}\,cm^{-2}$. Results on proton-induced damage in the crystal and its spontaneous recovery after both irradiations are presented here, along with some new, complementary data on proton-damage in lead tungstate. A comparison with FLUKA Monte Carlo simulation results is performed and a qualitative understanding of high-energy damage mechanism is attempted.

1. Introduction

The Large Hadron Collider (LHC) at CERN is expected to undergo a substantial upgrade in luminosity after the exploitation of its physics potential, to allow further exploration of the high-energy frontier in particle physics. The higher luminosity will strengthen the requirements on performance of most detector components. With data taking extended over several years under an increased luminosity, detectors will be exposed to even larger ionising radiation and hadron fluences than at the LHC, and they will need to be upgraded as well. While the harvest of LHC proton–proton collision data is just starting, studies are already being performed on a LHC upgrade (superLHC) where calorimetry will have to perform adequately in a radiation environment and hadron fluences an order of magnitude more severe than at the LHC. It will thus be important to have results at hand on calorimetric materials able to withstand the anticipated radiation levels and particle fluences before making decisions on detector upgrades.

Concerning hadron effects on crystals used for calorimetry, the present study extends to cerium fluoride (CeF_3) and complements our earlier work performed on lead tungstate ($PbWO_4$) [1–3]. In our earlier investigations we have shown that high-energy protons [1] and pions [2] cause a permanent, cumulative loss of light transmission in $PbWO_4$, while we observed no hadron-specific change in scintillation emission [3]. The features of the observed damage hint at disorder that might be caused by fragments of heavy elements, Pb and W. Above a certain threshold, these can have a range up to 10 μm and energies up to ~100 MeV, corresponding to a stopping power four orders of magnitude higher than the one of minimum-ionising particles. The associated local energy deposition is capable of inducing the displacement of lattice atoms.

The qualitative understanding we gained of hadron damage in lead tungstate lead us to predict [4] that such hadron-specific damage contributions are absent in crystals, like cerium fluoride, consisting only of elements with $Z < 71$, which is the experimentally observed threshold for fission [5]. Studies on cerium fluoride are expected to help at the same time in understanding hadron damage effects on scintillating crystals and possibly in providing a viable material for calorimetry in an extreme environment as the superLHC will be.

2. Cerium fluoride

Cerium fluoride is a scintillating crystal whose luminescence characteristics are known since the early studies by Kröger and Bakker [6], who measured its emission spectrum and light decay time constants and understood the responsible transitions. Its properties as a scintillator were revealed by Anderson [7] and by Moses and Derenzo [8], who attracted attention to its

* Corresponding author. Postal address: CERN PH Department, 1211 Geneva 23, Switzerland. Tel.: +41 22 767 6931; fax: +41 22 767 7971.
E-mail address: Francesca.Nessi-Tedaldi@cern.ch (F. Nessi-Tedaldi).
[1] Now at Massachusetts Institute of Technology, Cambridge, Massachusetts, USA.

0168-9002/$ - see front matter © 2010 Elsevier B.V. All rights reserved.
doi:10.1016/j.nima.2010.07.052

characteristics as a fast, bright and dense calorimetric medium for high-energy physics and positron-emission tomography applications.

Its density ($\rho = 6.16\,g/cm^3$), radiation length ($X_0 = 1.68\,cm$), Molière radius ($R_M = 2.6\,cm$), nuclear interaction length ($\lambda_I = 25.9\,cm$) and refractive index ($n = 1.68$) make it a competitive medium for compact calorimeters. Its emission is centred at 340 nm, with decay time constants of 10–30 ns; it is insensitive to temperature changes (dLY/dT(20 °C)=0.08%/°C) as well as bright (4–10% of NaI($T\ell$)) and thus suitable for high-rate, high-precision calorimetry [9].

In the nineties, this material was subject to an intense research program, that established its scintillation characteristics, its behavior in γ [10,11] and MeV-neutron irradiations [12] and the capability for crystal growers to produce crystals of dimensions suitable for high-energy physics applications. It should be noted that cerium is a readily available rare earth, which would allow containing raw material costs, were a mass production envisaged. Its melting point of 1430 °C allows applying well-known crystal growth technologies. The ability to grow crystals beyond 30 cm length was demonstrated, as visible in Fig. 1, but for its use in a calorimeter, R&D would have to be resumed, since no commercial production of macroscopic crystals presently exists, although the material is still used, e.g. in the form of 10 μm nanoparticles, for neutron capture cross-section measurements [13].

The tysonite structure is complicated, with each cerium atom surrounded by 11 fluorines in Edshammar's polyhedron [14] and the lower symmetry thus causes difficulties in the calculation of energy levels and defect structures [15]. Cerium fluoride is superionic [16], the fluorine ions having high mobility, which could account for part of its observed radiation hardness. It is also paramagnetic, a characteristics which influences the Faraday rotation in a magnetic field [17]. Fluorine ions labelled F_1 in the literature [18] account for most of the cerium fluoride conductivity and hence their mobility might help repair defects. There is a vast literature on this and in particular on doping [19] with barium and strontium, which have been observed to increase the conductivity even further [20]. The composition which maximizes conductivity might maximize radiation hardness as well, as hypothesised in Ref. [21], but establishing this would require a dedicated R&D. It should also be noticed that the cerium fluoride conductivity increases by a factor 4 between 20 and 50 °C [21], while its light output remains unaffected. Thus, for calorimetry applications in a hostile radiation environment, maintaining the crystals at a higher temperature could help minimising radiation damage. It is also pointed out in Ref. [21] that such crystals are the best fluoride superionics for electro-chemical solid state devices such as fuel cells.

The performance of cerium fluoride was also studied with high-energy particle beams in prototype crystal matrices [22], in particular since it was adopted as baseline calorimetric medium in the CMS [23] and L3P [24] Letters of Intent. Energy resolutions of the order of 0.5% for electron energies of 50 GeV and higher were achieved, and it was observed how cerium fluoride appeared to be the best material at that time for homogeneous electromagnetic calorimetry at LHC and only the need for a very compact calorimeter justified relegating it behind lead tungstate as the preferred material.

Cerium fluoride was also considered for the ANKE spectrometer upgrade at COSY and for medical imaging applications [25]. In Ref. [26], its energy response to electromagnetic probes was extended down to a few MeV in photon energy and a good time resolution, below 170 ps, was obtained using a time-of-flight technique.

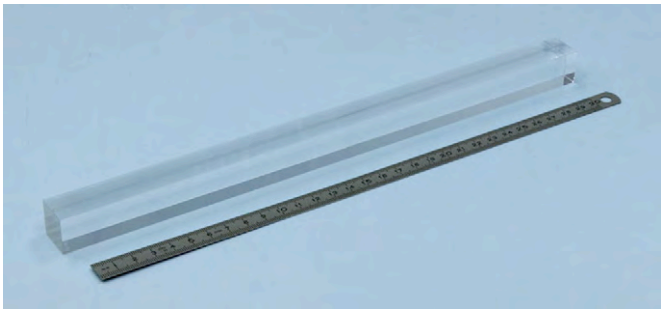

Fig. 1. A CeF_3 crystal, 30 cm long, produced by the Shanghai Institute of Ceramics.

3. Experimental setup

For this study, we have used a barium-doped CeF_3 crystal from Optovac [27], which has parallelepipedic shape with dimensions $21 \times 16 \times 141\,mm^3$ (8.4 X_0). The crystal was irradiated with 24 GeV/c protons at the IRRAD1 facility [28] in the T7 beam line of the CERN PS accelerator. The proton beam was broadened to cover the whole crystal front face, and the fluence for each irradiation was determined following the method described in Ref. [1], from the activation of an aluminium foil covering the crystal front face. The crystal was brought into the beam by a remotely controlled shuttle, and the irradiation was performed with the proton beam parallel to the long crystal axis.

The first irradiation was performed beginning of November 2007, with a flux $\phi_p = 1.16 \times 10^{12}\,cm^{-2}\,h^{-1}$. The proton fluence reached was $\Phi_p = (2.78 \pm 0.20) \times 10^{13}\,cm^{-2}$. After one year of periodic measurements, where its spontaneous recovery at room temperature, in the dark, was tracked, a second irradiation was carried out on the same crystal. Using the same crystal was intended to keep contributions from differences in geometry and in intrinsic characteristics nearly the same. During the second irradiation the proton flux was $\phi_p = 0.94 \times 10^{13}\,cm^{-2}\,h^{-1}$ and the proton fluence reached was $\Phi_p = (2.12 \pm 0.15) \times 10^{14}\,cm^{-2}$. Again, a similar series of measurements was performed over one year.

4. Results and discussion

4.1. Light transmission measurements

Longitudinal transmission (LT) curves before irradiation and at various intervals after proton irradiation are represented in Fig. 2. In the longitudinal light transmission before irradiation one observes that the smoothness of the transmission curve is interrupted by several dents which are known to be due to the presence of Nd^{3+} impurities [29] and are of no further concern to the present study, as explained later in this section. One also observes, in the light of Fig. 2 in Ref. [29], how the barium doping affects the optical absorption edge which sits right above 300 nm, i.e. ~15 nm higher compared to crystals grown with undoped raw material.

The earliest LT curves after irradiation were taken as soon as it was possible to handle the crystal while keeping people's exposure to radiation within regulatory safety limits, 18 days after the first irradiation and 62 days after the second one. From the LT curves, it is evident that the damage reduces light transmission at all wavelengths, while no transmission band-edge shift is observed after irradiation.

The extreme steepness of the band-edge, which is preserved throughout the proton irradiations, is due to an allowed transition, as indicated in Ref. [30], while the absence of a

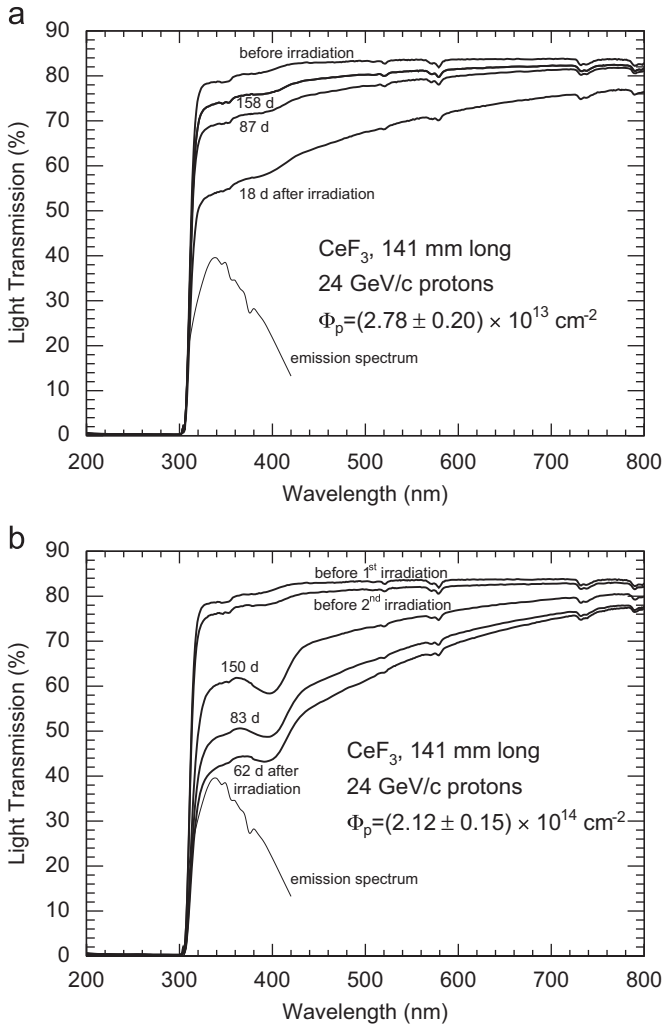

Fig. 2. Transmission curves for cerium fluoride before and at various times after the first irradiation (a) and before and at various times after the second irradiation (b). The emission spectrum is taken from Ref. [29] and has arbitrary normalisation.

band-edge shift in cerium fluoride is consistent with our predictions [4]. In fact, transmission measurement results in lead tungstate [1] and BGO [31] after hadron irradiation, had led us to argue [32] that the transmission band-edge shift observed in those crystals must be due to the disorder left by heavy fragments, causing an Urbach-tail behavior [33,34], and we had then further predicted [4] the absence of such a band-edge shift in crystals composed by elements with $Z<71$, where fission is not expected [5], as it is the case for cerium fluoride.

The longitudinal light transmission was repeatedly measured over time, to collect recovery data. The damage is quantified through the induced absorption coefficient as a function of light wavelength λ, defined as

$$\mu_{IND}(\lambda)=\frac{1}{\ell}\times\ln\frac{LT_0(\lambda)}{LT(\lambda)} \quad (1)$$

where LT_0 (LT) is the longitudinal transmission value measured before (after) irradiation through the length ℓ of the crystal.

Fig. 3 shows the profile of induced absorption as a function of wavelength, 150 days after each irradiation. We notice here the absence of the λ^{-4} behavior we previously observed [1] in lead tungstate. That behavior, peculiar to Rayleigh scattering, is a qualitative indication of the presence of very small regions of severe damage, as one expects to be caused by highly ionising

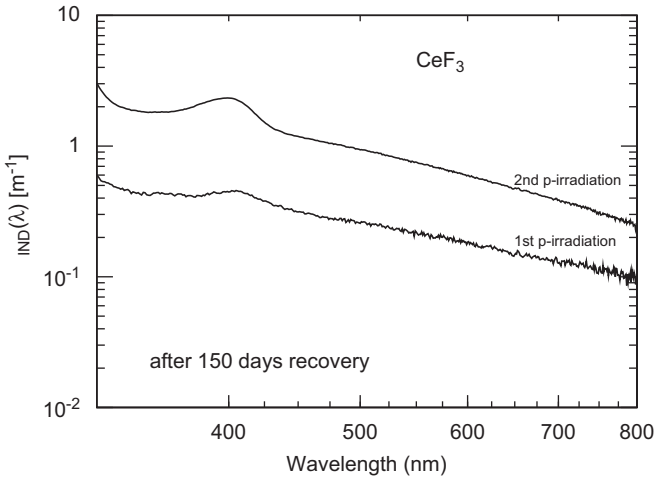

Fig. 3. Induced absorption coefficient as a function of wavelength in cerium fluoride, 150 days after each proton irradiation.

fragments from nuclei break-up. The absence of a Rayleigh-scattering behavior in cerium fluoride is a further confirmation of our understanding.

We also observe the presence of a yet unidentified absorption band, peaked around 400 nm, which does not recover with time, but is of no further concern for calorimetric applications, because it affects only a small fraction of the emitted light. It might be useful nevertheless, for any future detailed studies, to notice that the amplitude of this absorption band scales in a way which is consistent with a linear dependence on Φ_p. The density of centres N multiplied by the oscillator strength f calculated according to Ref. [35] for the second irradiation is

$$N\times f\simeq 1.7\times 10^{13}\,\mathrm{cm}^{-3}. \quad (2)$$

A FLUKA [36,37] simulation of the irradiation, which is described in detail in Section 4.3, yields an abundance $\rho=2.4\times10^{-2}\,\mathrm{cm}^{-3}$ of stable light nuclei (H and He) per impinging proton. Even assuming an oscillator strength $f=1$, such an abundance does not account for the observed absorption band, and thus allows to exclude defects caused by hydrogen and helium. Typical f-values range from 1 to 10^{-3} and therefore we hypothesise that the observed absorption band might be linked to defects in the cerium sub-lattice. In Ref. [29] it has been observed that an absorption band around that wavelength can be induced by ionising radiation and it was linked to the presence of fluorine vacancies and impurities. It shall be recalled here that hadronic showers induced by 24 GeV/c protons are a mixed field of secondary particles and ionising radiation, and thus the induced absorption we observe might well be linked to the mechanism above. Absorption bands at a lower wavelength, as observed in Ref. [38] for crystals of poor quality and linked therein to O^{-2} entrance, lie too far in wavelength to offer an explanation for our observations. Disentangling the various contributions to the observed spectrum of induced absorption coefficients as a function of wavelength would be an interesting subject of a further, extensive series of tests.

In Fig. 3, one also observes how the dips due to Nd^{3+} contamination, visible in the LT curves of Fig. 2 and mentioned earlier in the text, disappear when the induced absorption coefficients are evaluated. This proves that such dips are not influenced by radiation, nor are hidden absorption bands present underneath them.

After examining the overall proton-induced LT changes as a function of wavelength, in the following discussion we focus on

changes in longitudinal transmission at a wavelength of 340 nm, where the CeF_3 scintillation light emission reaches a maximum in intensity. The reason is, that changes at this wavelength where those which mostly affect the collection of the light that is used as a measure of particle energy deposition in calorimetric applications.

The evolution of damage over time is shown in Fig. 4 for the two irradiations, where $\mu_{IND}(340\,\text{nm})$ is plotted over time. The data, taken over one year, are well fitted by a sum of a constant and two exponentials with time constants $\tau_i (i=1,2)$

$$\mu^j_{IND}(340\,\text{nm}, t_{\text{rec}}) = \sum_{i=1}^{2} A^j_i e^{-t_{\text{rec}}/\tau_i} + A^j_3 \quad (3)$$

where t_{rec} is the time elapsed since the irradiation, while $A^j_i (i=1,2)$ and A^j_3 are the amplitude fit parameters for the irradiation $j (j=1,2)$. Fig. 4 shows a fit where the recovery time constants have been independently fitted for the two irradiations. The time constants obtained are compatible, yielding values $\tau_1 = 11 \pm 2$ days and $\tau_2 = 70 \pm 9$ days. Such a result is very important if one considers cerium fluoride for superLHC calorimetry: the contribution to the damage build-up during superLHC operation is smaller compared to the cumulative damage amplitude observed for lead tungstate [1]. In all this it should be pointed out, however, that our measurements are not sensitive to damage with a recovery time constant shorter than a few days, because the proton-irradiated crystal was initially too radioactive for safe handling during the first two weeks after irradiation, and thus no measurements were performed on it.

The dependence of damage on proton fluence is plotted in Fig. 5, in comparison with the values obtained for lead tungstate. The line therein is the fit from Fig. 15 in Ref. [1] to $\mu_{IND}(420\,\text{nm})$ for lead tungstate, 150 days after irradiation. The white circles are measurements of $\mu_{IND}(420\,\text{nm})$ for the same lead tungstate crystals studied in Ref. [1], taken 300 days after irradiation, showing how stable the long-term damage is in that crystal. Since in Ref. [1] all crystals studied were produced by the Bogoroditzk Techno-Chemical Plant (BTCP) in Russia, we have performed an irradiation of a further crystal produced by a different supplier, the Shanghai Institute of Ceramics (black circle in Fig. 5). The measurement for the SIC lead tungstate crystal is in perfect agreement with those for BTCP crystals, proving how hadron damage is not linked to fine details of doping, stoichiometry and intrinsic defects, nor to growth technology, but it is rather due to the effects induced by the hadron cascade in the bulk of the crystal.

It should be pointed out that all crystals tested in Ref. [1] are 23 cm (25.8 X_0) long, while the cerium fluoride crystal studied here is only 14.1 cm (8.4 X_0) in length. In the same plot, we have thus also superposed the proton damage measured in two lead tungstate crystals 7.5 cm (8.4 X_0) long, studied in Ref. [2] after a proton irradiation where they were placed one behind the other. Also for these shorter crystals $\mu_{IND}(420\,\text{nm})$ is well consistent with the values measured for the longer crystals. This can be understood from the star density profiles for 20–24 GeV/c protons in Fig. 3 of Ref. [1], which are nearly flat over the length of the crystal, besides a small build-up over the initial 5 cm, which is reflected in a slightly smaller damage in one of the two crystals. Thus, it appears justified to compare damage measured in an 8.4 X_0 long cerium fluoride crystal with the existing measurements for 23 cm long lead tungstate crystals. The induced absorption $\mu_{IND}(340\,\text{nm})$ at the peak of scintillation emission measured in cerium fluoride 300 days after irradiation is also plotted in Fig. 5. As easily understandable, a cumulative damage in cerium fluoride

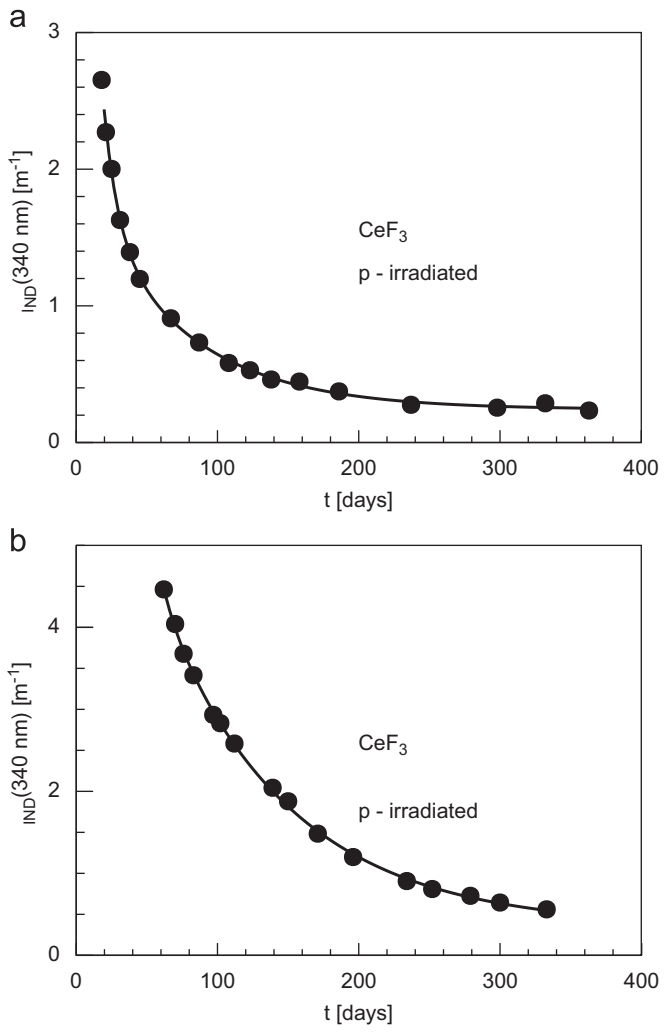

Fig. 4. Recovery curves for cerium fluoride after the first (a) and after the second (b) proton irradiation.

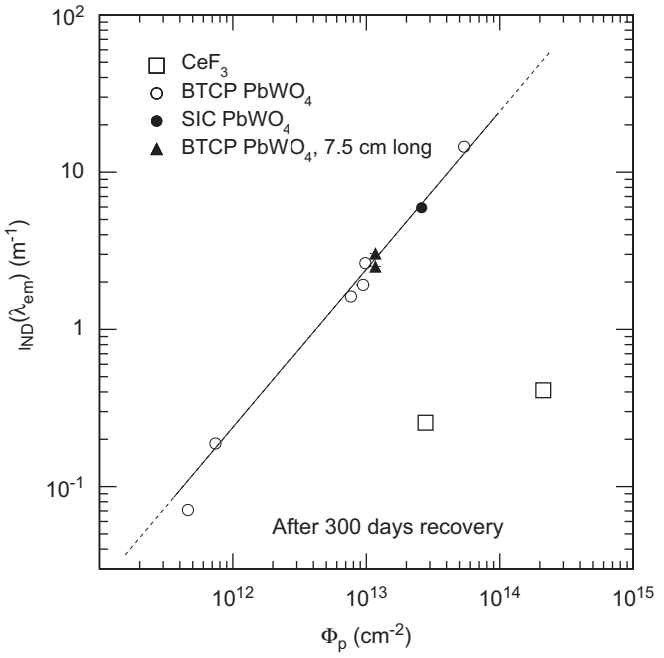

Fig. 5. Induced absorption coefficient versus proton fluence for cerium fluoride and for lead tungstate crystals of different length and origin.

would be fitted by a line parallel to the one for lead tungstate in this doubly logarithmic plot, which is not what we observe.

With the correlation of Fig. 5 extending over almost three orders of magnitude in fluence, the damage observed in cerium fluoride is not cumulative, and rather hints towards saturation. The amplitude observed 150 days after irradiation is a factor 15 smaller in cerium fluoride than in lead tungstate for a fluence $\Phi_p = 2.78 \times 10^{13}\,\mathrm{cm}^{-2}$ and a factor 30 smaller for $\Phi_p = 2.12 \times 10^{14}\,\mathrm{cm}^{-2}$. The gap increases to a factor 25 and 124, respectively, 300 days after irradiation, as also visible in Fig. 5. However, one has to be aware of the fact that the gap would be reduced by a factor 1.5, were the induced absorption expressed in units of inverse radiation length.

In our understanding, the fact that the long-term proton-induced absorption in cerium fluoride is more than one order of magnitude smaller than in lead tungstate and is not cumulative, is linked to the absence of a damage mechanism related to fission fragments. The induced absorption in cerium fluoride after proton irradiation recovers at room temperature, and has a modest amplitude that makes this crystal very suitable for a harsh environment as will be calorimetry at superLHC. The observed changes might be due to the ionising dose accompanying the protons, or to secondaries, like neutrons (see, e.g. [12]) produced in the hadronic shower. A detailed understanding of the involved mechanisms would require performing an extensive series of tests under gamma, neutron, proton and pion irradiation, that could only be performed in collaboration with crystal growing partners. Furthermore, a systematic study of hadron effects on cerium fluoride crystals of different quality should be envisaged before starting a mass production of crystals to be used in an environment where hadron effects can be important.

4.2. Light output measurements

The relevant quantity for calorimeter operation is the Light Output (LO), and thus, in the present study we have verified that with the recovery of light transmission, also the light output is restored. For this purpose, we have acquired light output spectra using a bialkaline 12-stage photomultiplier (PM), and we have digitized its anode charge using a charge-integrating ADC as described in Ref. [3].

To identify a scintillation signal well above the background due to the intrinsic induced radioactivity after proton irradiation, we have triggered on cosmic muons traversing the crystal sideways, by means of two plastic scintillators. Such muons are minimum-ionising, and leave, according to Ref. [39], an energy deposit of 7.9 MeV/cm in the crystal. Due to the geometrical acceptance of the trigger scintillator setup, the mean path in the crystal is 2.3 ± 0.2 cm and thus the muon energy deposit in average is 18.2 ± 1.6 MeV. The photomultiplier signals were attenuated by 26 db before digitization, to match the dynamic range of the ADC. The resulting light output spectrum, which is analogous to the one we observed in lead tungstate (Fig. 1 in Ref. [3]), is shown in Fig. 6, where the peak of the cosmic muon energy deposit distribution is determined to be centred at channel 1276 ± 8. The leftmost part of the spectrum is not shown, to suppress the sharp rise at low channel values, due to light produced by the radioactivity of the crystal causing accidental coincidences when triggering on cosmic muons.

To study in detail the contribution of intrinsic radioactivity to the energy deposition spectrum in the crystal, we have furthermore acquired the spectrum shown in Fig. 7, using 0 db attenuation and the same PM gain as above. There, we triggered on the light output from the crystal itself using a threshold set below the level of single photoelectrons thermally emitted by the photocathode: those yield the leftmost peak in the histogram. The peak at channel 225 ± 1 corresponds, if we determine its equivalent energy deposit scaling from the muon peak position, to $E_\gamma = 160 \pm 10$ keV. As it will be evident from activation measurements and related FLUKA simulations described in the following sections, the dominant isotope created in the proton irradiation tests is ^{139}Ce, whose electron capture decay to ^{139}La is accompanied by an emission of a 165 keV photon. The peak we observe in the spectrum is in good agreement with the activity from this isotope.

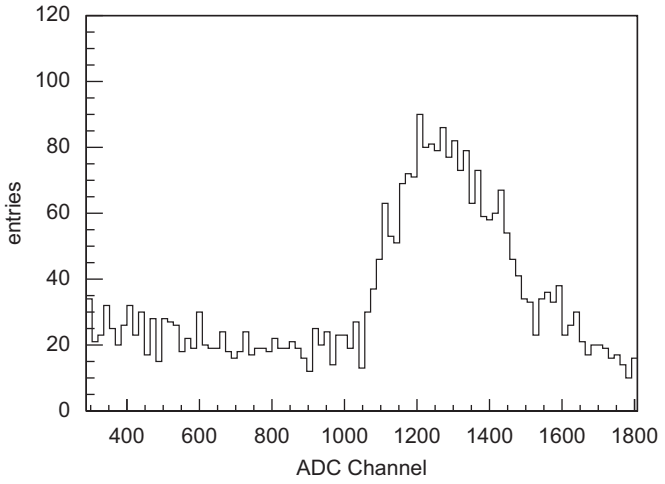

Fig. 6. Pedestal-subtracted scintillation spectrum in proton-irradiated cerium fluoride, showing the peak due to cosmic muons, taken with 26 db attenuation on the signal input to the ADC, and triggering with plastic scintillators as described in the text.

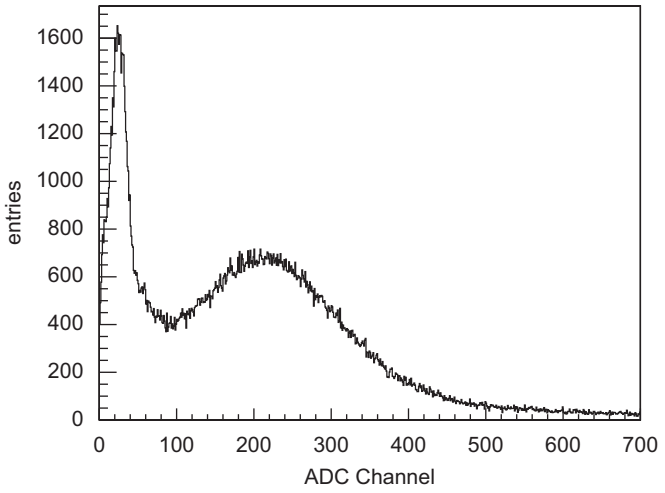

Fig. 7. Pedestal-subtracted scintillation spectrum in proton-irradiated cerium fluoride, showing a peak possibly due to ^{139}Ce, taken with 0 db attenuation on the signal input to the ADC, while triggering on signals from the crystal itself.

A light output measurement using cosmic muons one year after the second irradiation allows us to determine a remaining loss of $\Delta LO/LO = (11 \pm 2)\%$. The measured fraction of induced absorption coefficient which has not recovered one year after the second irradiation (see Fig. 5), is $\mu_{IND} = 0.33 \pm 0.04\,\mathrm{m}^{-1}$. A correlation between LO loss and induced absorption has been published in Ref. [3] for 23 cm long lead tungstate crystals, and the correlation therein between LO loss and induced absorption coefficients is similar to the one we observe here. A precise comparison would require taking into account the different crystal dimensions and their influence on light collection. Our

measurement however shows how the observed spontaneous recovery at room temperature of light transmission after hadron irradiation in cerium fluoride up to $\Phi_p = (2.12 \pm 0.15) \times 10^{14}\,\mathrm{cm}^{-2}$ is accompanied, as expected, by an almost complete recovery of scintillation light output.

4.3. Activation measurements

4.3.1. Present irradiations

Hadron irradiation causes the production of radioactive isotopes in the crystals. While most of them are short-lived, those with a long half-life are responsible for the remnant radioactivity and are relevant in case a calorimeter needs human intervention after exposure. It might thus be of interest to compare measurements of radio-activation in cerium fluoride to those in lead tungstate. The latter has been extensively studied through simulations and measurements in our early work [1] and references therein. The measurements there agree with simulation results on average within 30% and never beyond a factor of 2, and confirm that radiation exposure is an important concern for a lead tungstate calorimeter used in intense hadron fluences. Activation measurements in cerium fluoride provide an important practical information on access and handling possibilities for such a calorimeter if used at superLHC. The induced ambient dose equivalent rate ("dose") $\dot{H}^*(10)_{\mathrm{ind}}$ was regularly measured according to the procedure described in Ref. [1] with an Automess 6150AD6 [40] at a distance of 4.5 cm from the long face of the crystal at its longitudinal centre. The reference point of the sensitive element in the 6150AD6 is reported to be 12 mm behind the entrance window. Thus our actual distance was 5.7 cm from the crystal face. The measured dose as a function of cooling time is plotted in Fig. 8. The activation values are compatible with the scaling of fluences, if one takes into account that when the second irradiation was started, the crystal was still showing a remaining level of activation from the first one.

We have fitted the data, taken over one year, with a sum of a constant and two exponentials with time constants $\tau_i (i = 1,2)$

$$\dot{H}^*(10)_{\mathrm{ind}}(t_{\mathrm{rec}}) = \sum_{i=1}^{2} D_i^j e^{-t_{\mathrm{rec}}/\tau_i} + D_3^j \tag{4}$$

where t_{rec} is the time elapsed since the irradiation, while $D_i^j, (i = 1,2)$ and D_3^j are the amplitude fit parameters for irradiation $j (j = 1,2)$. The time constants obtained for the two independent fits are compatible, with values $\tau_1 = 11$ days and $\tau_2 = 85$ days. Interestingly, the radio-activation recovery time constants are compatible within 2σ with those for the damage recovery determined in Section 4.1. While there is no evidence for a link between the two, we wonder whether the long-lived induced absorption component might be due to a self-irradiation of the crystal. Further studies would be worthwhile to understand such effects and possibly establish this link.

FLUKA Monte Carlo simulations were performed using the code Version 2008.3c.0 [36,37] and rely on the input parameters used in our $PbWO_4$ study [41,1]. The beam profile was assumed to be squared ($3 \times 3\,\mathrm{cm}^2$) and uniformly distributed. The crystal was simulated according to the experimental setup. The FLUKA geometry includes also the back wall of the irradiation zone, i.e. the T7 beam line dump. Because the hadron shower induced by beam protons impinging on the crystal shows a significant forward direction, such that the integrated hadron fluence at the backside is roughly 10 times more intense than the lateral fluence, the side walls were neglected.

For the dose measurements following the irradiation, the crystal has been removed from the irradiation zone and was kept for measurements in an area with low background. To simulate

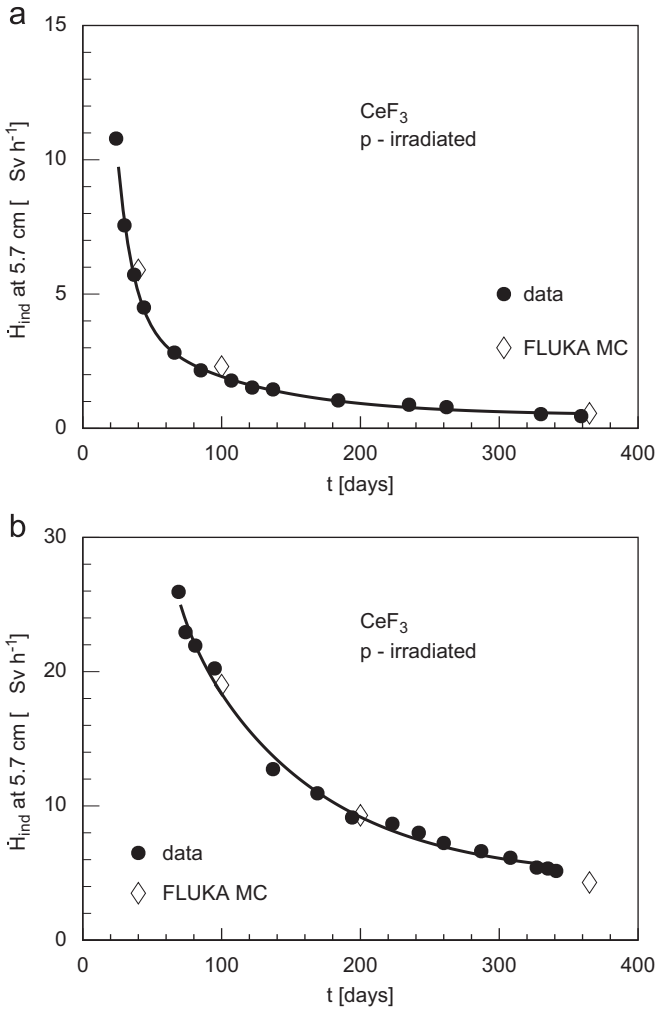

Fig. 8. Measured remnant dose (black dots) as a function of cooling time for cerium fluoride after the first irradiation (a) and after the second irradiation (b) compared to the expected values from FLUKA simulations (white lozenges).

the two processes with different geometries, the FLUKA two-step method [42] was applied. In a first step (the irradiation) the produced radionuclides in the crystal, namely the γ- and β^+−emitters, were recorded. These provided the input for the second step, where the average ambient dose equivalent to a volume of $1\,\mathrm{cm}^3$ was calculated, using fluence to ambient dose equivalent conversion coefficients [43]. The centre of the dose recording region was set laterally centred and at a distance of 5.7 cm from the crystal, according to the experimental settings. The FLUKA simulation results of the cerium fluoride activation at a few intervals after each of the two irradiations are shown in Fig. 8. One approximation was made in the simulation: a single irradiation was assumed in each case, while the same crystal was actually irradiated twice at one year's interval. This might explain the slight dose underestimate from FLUKA at long cooling times after the second irradiation. Table 1 lists the isotopes expected to be still present in the crystal, according to FLUKA, one year after the irradiation up to a fluence $\Phi_p = 2.78 \times 10^{13}\,\mathrm{cm}^{-2}$ and with an activity larger than $10\,\mathrm{Bq/cm}^3$. From the tabulated values, it is evident that the isotope that contributes with the largest activity is ^{139}Ce. One may also notice that the longer recovery time constant fitted in Fig. 8 for the radiation dose is of the same order of magnitude as the life time of ^{139}Ce. Taking into account

Table 1
Dominating isotope activities in cerium fluoride from FLUKA simulations, one year after irradiation by 24 GeV/c protons up to a fluence $\Phi_p = 2.78 \times 10^{13}$ cm^{-2}.

Isotope	$\tau_{1/2}$	Activity (Bq/cm^3)	Total γ energy(MeV)
^{3}H	12.33y	1017 ± 3	–
^{88}Y	106.65d	109 ± 1	2.734
^{109}Cd	462.6d	114 ± 1	0.088
^{139}Ce	137.64d	930 ± 6	0.166

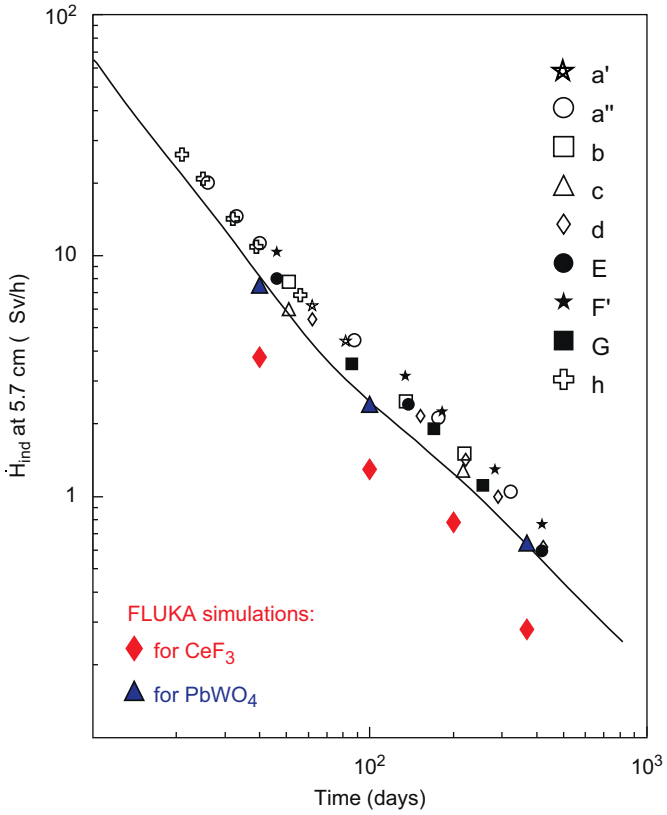

Fig. 9. FLUKA simulation of a 42 cm long CeF_3 crystal remnant dose as a function of cooling time (full lozenges), compared to data (symbols) and simulation (line) results on 23 cm long lead tungstate crystals from Ref. [1] for a fluence $\Phi_p = 10^{13}$ cm^{-2} of 20 GeV/c protons. Full triangles indicate, for validation purposes, our simulation results for lead tungstate.

contributions from the other long-lived isotopes present, the agreement is quite reasonable.

4.3.2. *Full-size crystals*

A comparison between cerium fluoride and lead tungstate activation levels after hadron irradiation for full-size crystals is a relevant input to the selection of the calorimetric medium for a calorimeter upgrade. In Fig. 9, we show the results from our FLUKA simulation for the irradiation and cooling conditions of Ref. [1] for full-size lead tungstate crystals exposed to 20 GeV/c protons, compared to the measured activation and the FLUKA simulation performed therein. The agreement validates the present FLUKA simulations. The FLUKA results for the activation expected for full-size cerium fluoride crystals are also shown in Fig. 9. Because of the smaller density and longer radiation length of cerium fluoride, a full-size calorimeter crystal would have to be 42 cm in length. Transverse dimensions of 24 mm × 24 mm correspond to the typical cross-section yielding a similar $\eta-\phi$ granularity as for existing lead tungstate calorimeters. The FLUKA simulation, which was validated already for short cerium fluoride crystals (Fig. 8) and for lead tungstate (Fig. 9), was performed for such full-size dimensions and for the same fluence of $\Phi_p = 1 \times 10^{13}$ cm^{-2}, yielding dose values shown as lozenges in Fig. 9. One observes that workers' exposure to proton-irradiated, 26 X_0 long cerium fluoride crystals is expected to be always a factor of 2–3 lower than the one due to lead tungstate.

5. Conclusions

We have studied cerium fluoride as a possible scintillating crystal for calorimetry at the superLHC. This investigation was inspired by our earlier studies of lead tungstate, where we observed a hadron-specific, cumulative damage from charged hadrons. All characteristics of the damage in lead tungstate are consistent with an intense local energy deposition from heavy fragments. Measurements of absorption induced in CeF_3 by 24 GeV/c protons up to fluences $\Phi_p = (2.78 \pm 0.20) \times 10^{13}$ cm^{-2} and $\Phi_p = (2.12 \pm 0.15) \times 10^{14}$ cm^{-2} show a light transmission damage which is not cumulative, is more than one order of magnitude smaller than in $PbWO_4$ 6 months after irradiation, and—unlike $PbWO_4$—recovers further. The absence of a dominant Rayleigh-scattering component in CeF_3 confirms our understanding, that in $PbWO_4$ it is due to highly ionising fission fragments as produced in crystals with elements above $Z=71$. The scintillation light output in CeF_3 is observed to recover by 90% over one year, and the remaining loss is consistent with the induced absorption still present, with no indication of a hadron-specific damage to the scintillation properties.

With its extreme resistance to hadron-induced damage, manifested through a modest induced absorption which recovers with time, low raw material costs, high light yield and negligible temperature dependence, cerium fluoride is an excellent candidate for medical imaging applications and for calorimetry at superLHC or in any high hadron fluence environment.

Acknowledgements

We are indebted to R. Steerenberg, who provided us with the required CERN PS beam conditions for the proton irradiations. We are deeply grateful to M. Glaser, who operated the proton irradiation facility and provided the Aluminium foil dosimetry.

References

[1] M. Huhtinen, P. Lecomte, D. Luckey, F. Nessi-Tedaldi, F. Pauss, Nucl. Instr. and Meth. A 545 (2005) 63.
[2] P. Lecomte, D. Luckey, F. Nessi-Tedaldi, F. Pauss, D. Renker, Nucl. Instr. and Meth. A 587 (2008) 266.
[3] P. Lecomte, D. Luckey, F. Nessi-Tedaldi, F. Pauss, Nucl. Instr. and Meth. A 564 (2006) 164.
[4] F. Nessi-Tedaldi, J. Phys. Conf. Ser. 160 (2009) 012013.
[5] A.S. Iljinov, M.V. Mebel, C. Guaraldo, V. Lucherini, E. De Sanctis, N. Bianchi, P. Levi Sandri, V. Muccifora, E. Polli, A.R. Reolon, P. Rossi, S. Lo Nigro, Phys. Rev. C 39 (1989) 1420.
[6] F.A. Kröger, J. Bakker, Physica VIII (1941) 628.
[7] D.F. Anderson, IEEE Trans. Nucl. Sci. NS-36 (1989) 137.
[8] W.W. Moses, S.E. Derenzo, IEEE Trans. Nucl. Sci. NS-36 (1989) 173.
[9] D.F. Anderson, Nucl. Instr. Meth A 287 (1990) 606.
[10] M. Kobayashi, M. Ishii, E.A. Krivandina, M.M. Litvinov, A.I. Peresypkin, Yu.D. Prokoshkin, V.I. Rykalin, B.P. Sobolev, K. Takamatsu, V.G. Vasil'chenko, Nucl. Instr. and Meth. A 302 (1991) 443.
[11] S. Anderson, E. Auffray, T. Aziz, S. Baccaro, S. Banerjee, P. Bareyre, L.E. Barone, B. Borgia, D. Boutet, J.P. Burq, M. Chemarin, R. Chipaux, I. Dafinei, P. D'Atanasio, F. De Notaristefani, B. Dezillie, C. Dujardin, S. Dutta, J.L. Faure, et al., Crystal Clear Collaboration, Nucl. Instr. and Meth. A 332 (1993) 373.
[12] R. Chipaux, J.-L. Faure, P. Rebourgeard, G. Dauphin, J. Safieh, Nucl. Instr. and Meth. A 345 (1994) 440.

[13] S. Stange, E.I. Esch, A.J. Couture, R.E. Del Sesto, R.D. Gilbertson, T.M. McCleskey, E.A. McKigney, R.E. Muenchausen, R. Reifarth, Development of nanocomposite scintillators for neutron capture measurements, in: paper N25-115, IEEE/NSS 2009 Conference Record, 2009.
[14] B.G. Hyde, S. Anderson, Inorganic Crystal Structure, Wiley, New York, 1989.
[15] H. Merenga, Electronic structure calculations on cerium-containing crystals, Ph.D. Thesis, Delft University Press, NL, 1997.
[16] V. Trnovcova, L.S. Garashina, A. Skubla, P.P. Fedorov, R. Cicka, E.A. Krivandina, B.P. Sobolev, Solid State Ionics 157 (2003) 195.
[17] Y. Xu, M. Duan, Phys. Rev. B 46 (1992) 11636.
[18] S. Hull, Rep. Prog. Phys. 67 (2004) 1233.
[19] A. Roos, F.C.M. van de Pol, R. Keim, J. Schoonman, Solid State Ionics 13 (1984) 191.
[20] A.F. Privalov, I.V. Murin, Phys. Solid State 41 (1999) 1482;
D. Kruk, J. Phys. Condens. Matter 18 (2006) 1725.
[21] N.I. Sorokin, B.P. Sobolev, Crystallogr. Rep. 52 (2007) 842.
[22] E. Auffray, T. Beckers, J. Bourotte, R. Chipaux, V. Commichau, I. Dafinei, P. Depasse, L. Djambazov, U. Dydak, H. El Mamouni, J. Fay, M. Felcini, M. Goyot, M. Haguenauer, K. Hangarter, H. Hillemanns, H. Hofer, B. Ille, B. Jacobs, T. Kirn, P. Lebrun, P. Lecomte, P. Lecoq, J.P. Martin, M. Mattioli, G. Maurelli, I. Melnikov, F. Nessi-Tedaldi, L. Pacciani, S. Pirro, R. Raghavan, D. Ren, M. Reynaud, U. Ršser, P. Sahuc, D. Schmitz, M. Schneegans, J. Schwenke, I. Soric, G. Viertel, H.P. Von Gunten, J.P. Walder, S. Waldmeier-Wicki, Nucl. Instr. and Meth. A 378 (1996) 171.
[23] The CMS Collaboration, CMS Letter of Intent, CERN/LHCC 92-003, LHCC/I 1, CERN, Geneva, Switzerland, 1992.
[24] The L3P Collaboration, L3P Letter of Intent, CERN/LHCC 92-005, LHCC/I 3, CERN, Geneva, Switzerland, 1992.
[25] W.W. Moses, S. Derenzo, M.J. Weber, A.K. Ray-Chaudhuri, F. Cerrina, J. Lumin. 59 (1994) 89.
[26] R. Novotny, R. Beck, W. Dšring, V. Hejny, M. Hoek, A. Hofstaetter, V. Metag, K. Römer, Nucl. Instr. and Meth. A 486 (2002) 131.
[27] Optovac, North Brookfield, USA, later acquired by Corning Advanced Material, Corning, USA.
[28] M. Glaser, L. Durieu, F. Lemeilleur, M. Tavlet, C. Leroy, P. Roy, ROSE/RD48 Collaboration, Nucl. Instr. and Meth. A 426 (1999) 72.
[29] E. Auffray, S. Baccaro, T. Beckers, Y. Benhammou, A.N. Belsky, B. Borgia, D. Boutet, R. Chipaux, I. Dafinei, F. de Notaristefani, P. Depasse, C. Dujardin, H. El Mamouni, J.L. Faure, J. Fay, M. Goyot, S.K. Gupta, A. Gurtu, H. Hillemanns, B. Ille, et al., Nucl. Instr. and Meth. A 383 (1996) 367.
[30] M. Schneegans, Nucl. Instr. and Meth. A 344 (1994) 47.
[31] M. Kobayashi, K. Kondo, H. Hirabashi, S. Kurokawa, M. Taino, A. Yamamoto, S. Sugimoto, H. Yoshida, T. Wada, Y. Nakagawa, M. Ogawa, M. Ishii, S. Akiyama, H. Ishibashi, Nucl. Instr. and Meth. A 206 (1983) 107.
[32] G. Dissertori, D. Luckey, P. Lecomte, F. Nessi-Tedaldi, F. Pauss, Studies of hadron damage in lead tungstate and cerium fluoride crystals for HEP calorimetry, in: paper N55-1, IEEE/NSS 2008 Conference Record, 2008.
[33] F. Urbach, Phys. Rev. 92 (1953) 1324.
[34] M. Itoh, H. Yokota, M. Horimoto, M. Fujita, Y. Usuki, Phys. Stat. Sol. 231 (2002) 595.
[35] D.L. Dexter, Phys. Rev. 101 (1956) 48.
[36] A. Ferrari, P.R. Sala, A. Fasso, J. Ranft, FLUKA: a multi-particle transport code, CERN 2005-10, INFN TC 05/11, SLAC-R-773, 2005.
[37] G. Battistoni, S. Muraro, P. Sala, F. Cerutti, A. Ferrari, S. Roesler, A. Fasso, J. Ranft, The FLUKA code: description and benchmarking, in: Proceedings of the Hadronic Shower Simulation Workshop 2006, Fermilab 6–8 September 2006; R. Raja (Ed.), AIP Conf. Proc. 896 (2007) 31–49.
[38] G. Ming, F. Xiqi, H. Guanqin, Y. Zhiwen, Nucl. Instr. and Meth. A 348 (1994) 163.
[39] R.M. Barnett, et al., Phys. Rev. D 54 (1996) and references therein.
[40] Gebrauchsanweisung für den Dosisleistungsmesser 6150AD6, Automation und Messtechnik AG, Ladenburg, Germany, 2001.
[41] M. Huhtinen, CERN, Geneva, Switzerland, private communication.
[42] S. Roesler, M. Brugger, Y. Donjoux, A. Mitaroff, Simulation of remanent dose rates and benchmark measurements at the CERN-EU high-energy reference field facility, in: Proceedings of Sixth International Meeting on Nuclear Applications of Accelerator Technology, 1–5 June 2003, pp. 6555–6662.
[43] S. Roesler, G R. Stevenson, deq99.f—a FLUKA user-routine converting fluence into effective doseand ambient dose equivalent, CERN-SC-2006-070-RP-TN, 2006.